Chemical and Process Engineering: New Frontiers, 2025, 46(4), e106
DOI: 10.24425/cpe.2025.155544

Water acrylic emulsions with silver nanoparticles: Study on stability and thermomechanical properties

Anna Zalewska[1], Ireneusz Grubecki[2]

[1] Bydgoszcz University of Science and Technology, 3 Seminaryjna Street, 85-326 Bydgoszcz, Poland
[2] Cracow University of Technology, 24 Warszawska Street, 31-155 Krakow, Poland

*** Corresponding author, e-mail:**
anna.zalewska@pbs.edu.pl

Article info:
Received: 6 June 2025
Revised: 11 August 2025
Accepted: 10 September 2025

Abstract
Ecological painting materials are innovative products that are becoming more and more popular among producers and consumers. In the most common cases, scientists apply nanometals or their oxides, especially silver nanoparticles, which – thanks to their extraordinary properties – are widely used not only in the pharmaceutical, cosmetic industries as well as in (bio)medicine but also as a supplement to improve the properties of protective coatings, as has been shown in this paper. In particular the paper discusses the impact of silver nanoparticles content added to the water acrylic emulsions on their stability, expressed by Turbiscan Stability Index, and thermomechanical properties of coatings manufactured from them.
It was concluded that the addition of silver nanoparticles makes the dispersions more stable compared to those with no addition of silver nanoparticles. Furthermore, in the case of the coatings manufactured from the paint composition, the increase in the nanosilver particle content shifts the pour and softening points towards higher temperature values. As a consequence, the layers become less flexible.
The problem under consideration has relevant importance for the development of novel, environmentally friendly coatings applicable in various areas of life.

Keywords
water-based acrylic, silver nanoparticles, antibacterial coatings, stability, polymer dispersion

1. INTRODUCTION

Applicable legislation and growing consumer awareness of matters concerning health, potential risks to the environment, and the need to reduce fire risk prompted the need to reduce emissions of volatile organic compounds into the atmosphere. Hence, water based acrylic resins – which are an excellent alternative to solvent-borne systems of many types – can be used in the production of paints and varnishes due to significantly lower harmful impact on the environment compared to those based on organic solvents. Examples of these are water-based acrylic paints and varnishes, which owe their popularity to their decorative properties in addition to their protective properties. An aqueous polymer dispersion (binder) with high molecular weight polymer particles is the basic component of such products. Other, equally important components are present in addition to aqueous polymer dispersions, e.g., surfactants, pigments, fillers and auxiliary agents, whose contribution is necessary to obtain products with the required stability and performance properties. Hence, acrylic resin-based paint products are constantly being modified.

A significant impact of nanotechnology can be noted here. It exerts an evolving technology that has a huge impact on an extremely large number of industries (Kargozar and Mozafari, 2018; Piracha et al., 2021; Schaming and Remita, 2015; Sharma et al., 2022; Taran et al., 2021).

Researchers and manufacturers of painting products, looking for new solutions, use nanometals. It is the nanometric-size materials used in polymer compositions that result in significant improvements in their functional properties, finding applications in various industry sectors (Chinh et al., 2022; Sharma et al., 2022), including the production of paints and varnishes (Abdullayev et al., 2009; Akbarian et al., 2012; Gómez-Ortíz et al., 2013; Şen et al., 2022; Tornero et al., 2018; Zhang et al., 2021). In particular, it is worth mentioning that the COVID-19 pandemic has contributed to the development of new materials aimed at eliminating responsible pathogens (Assis et al., 2021).

Among the various types of nanoparticles, AgNPs have attracted considerable attention in various applications due to the nanosilvers' small size, large surface area, and optical properties – the ability of AgNPs to interact with light (Duman et al., 2024). Mostly, silver nanoparticles are employed as an agent indispensable for therapeutic applications in modern healthcare practice. This is because of their strong antibacterial properties due to their ability to bind to bacterial cell walls, disrupting their metabolic functions, blocking processes such as respiration and DNA replication, and destroying the structure of proteins, which leads to bacteria inactivation.

A graphical diagram of the exemplary applications of AgNPs in (bio)medical procedures is shown in Fig. 1 (Gherasim et al., 2020; Loiseau et al., 2019; Schluesener and Schluesener, 2013).

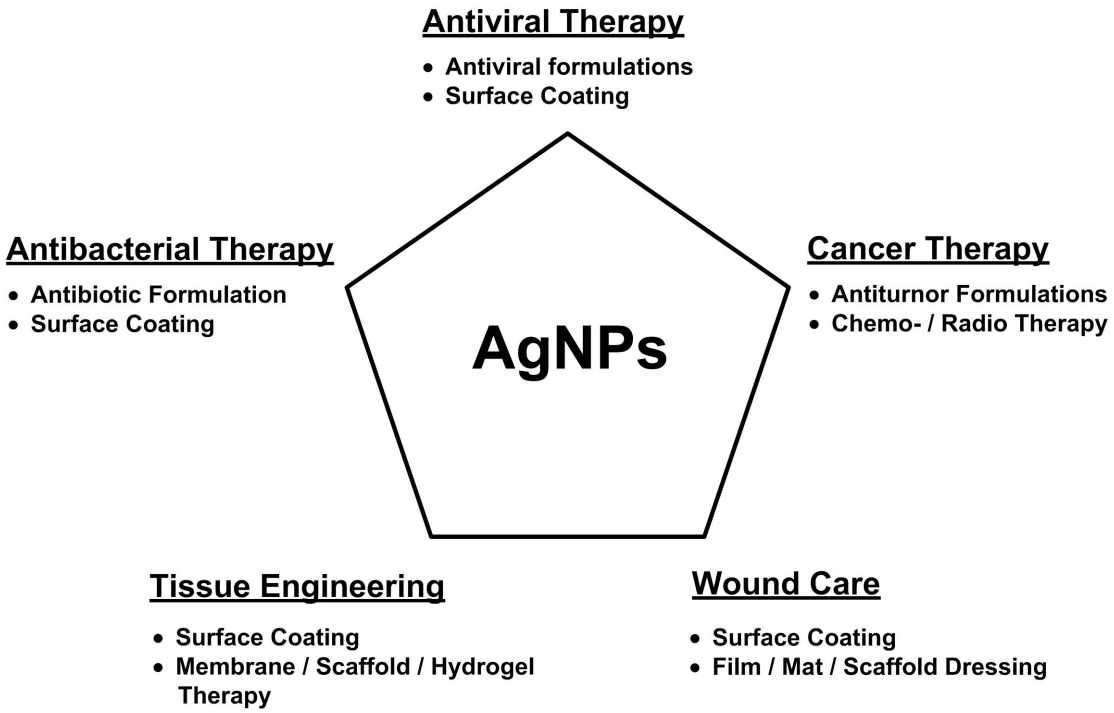

Figure 1. Exemplary applications of AgNPs in (bio)medical procedures.

Nanosilver particles engineered for specific purposes have significantly expanded the possibilities for their use beyond the realm of (bio)medicine. Owing to their physical properties, they are an attractive material for many industries, including (1) environmental protection, in removing or reducing contaminants in soil, and groundwater (Khan et al., 2023; Sharma et al., 2015); (2) electronics industry, in conductive inks, sensors, and coatings for electronics industry due to their enhanced conductivity (Loiseau et al., 2019; Wu et al., 2020); (3) cosmetics industry, in creams, lotions, and deodorants for their antimicrobial effects (Ong and Nyam, 2022); (4) food industry (Carbone et al., 2016); (5) chemical industry (Dhaka et al., 2023); (6) textile industry (Abazari et al., 2023; Shah et al., 2022); (7) biotechnology (Sarmast and Salehi, 2016), and (8) the manufacturing of paints and varnishes (Benitha et al., 2024).

From the viewpoint of the considerations presented in this work, the lattermost application is the object of special attention due to unique characteristics such as antimicrobial, anticorrosive, antiviral and dust-repellent properties (Manjumeena et al., 2016).

That is because – as above-mentioned – silver nanoparticles have the ability to destroy bacteria and fungi by interacting with their cell membrane and enzymes, efficiently leading to cell death. Therefore, AgNPs added to painting materials induce highly desirable properties, which makes them applicable in various sectors of every-day life, including:

- *healthcare facilities* – AgNPs effectively prevent various types of bacteria and fungi, which allows for a safer environment for patients and staff;
- *food industry and packaging* – in order to prevent microorganism growth as well as to extend product usability time;
- *household appliance* – AgNPs can be used to refine materials used in the production of equipment, for example refrigerators, to protect the surface from microorganism pollution, ensuring a more harmless environment for users;
- *civil engineering* – in order to guarantee high air quality indoor it is possible to apply the coatings with AgNPs to walls to prevent microorganism growth.

Consequently, by using AgNPs as a modifier of polymer compositions, manufacturers can produce coatings that inhibit microbial growth, ensuring a long-term safety, and reducing the frequency of renovations and their cost at the same time.

In addition to the properties provided by the coatings, the monitoring of changes taking place during storage and warehousing, i.e., stability, plays an important role in the practice of paint production.

Knowledge regarding the impact of changes in weather conditions on the properties of coatings is particularly crucial. Extremely low and/or high temperatures promote the formation of microcracks, which weaken the coating structure and increase its susceptibility to further damage, which may additionally lead to loss of adhesion.

In turn, in situations of high humidity, coatings with increased water resistance should be employed. Therefore, long-term effects of weather conditions such as moisture, salt and pollutants may lead to the development of corrosion, especially in places where the coating is damaged.

Hence, the challenge for engineers is to create products with good stability (Apelfeld et al., 2022). In order to achieve this, it is necessary to perform thermomechanical studies to evaluate the effect of temperature changes on the viscoelastic properties of polymer compositions. Knowledge of thermal stability in its broadest sense and the behaviour of materials in relation to temperature changes, accounting for thermal degradation problems, is a key factor in developing the most favourable composition from the perspective of coating behaviour in the conditions provided for their use.

In the present study, research was carried out to assess the stability of dispersions analysing the particle size distribution as well as thermomechanical and physical-mechanical properties of coatings manufactured of them. The research covered a dispersion system containing an acrylic resin enriched with Rokanol K-14, considered to be the surface active agent (SAA), colloidal silica (SiO_2) with AgNPs, the contents of which were analysed.

Differences in chemical composition, morphology, size, and controlled dispersity lead to variations in the properties of nanoparticles, especially silver nanoparticles. Smaller particles with a bigger surface area work better as antibacterials than larger ones because AgNPs can contact bacterial cells (Keijzer et al., 2022; Sati et al., 2025; Shahzadi et al., 2025). Therefore, the analysis presented in this study is fully justified, as the addition of AgNPs may lead to nanoparticle aggregation and system supersaturation, which in turn can reduce the stability of polymer dispersions and deteriorate the functional properties of the resulting coatings.

The use of surface active agent (SAA) and colloidal silica (SiO_2) as a carrier effectively prevent the aforementioned phenomena, contributing to the stability of the polymer dispersions developed in this study.

Colloidal silica of rough surface – after modifying the surface by silanization – to support AgNPs so that the ultra-fine AgNPs can be homogeneously formed without aggregation while giving mechanical interlocking, enhancing binding strength, and long-term, broadly understood stability of AgNPs which are crucial for their applications like antibacterial coatings (Hoang et al., 2020; Mousavi and Fini, 2020).

The analysed polymer composite is supposed to be applied to wooden furniture and metal surfaces, as equipment for hospitals, laboratories and housing (Le et al., 2019).

2. MATERIALS AND METHODS

2.1. Materials

In this study the following components were used:

- Alberdingk AC 3640 (acrylic resin): solids content 40–42%, pH 7.5–8.0, boiling point 373 K, Brookfield viscosity 50–500 mPa·s, relative density of 1000–1100 kg·m^{-3}, vapour pressure 2.3 kPa (293 K), (Alberdingk Boley);
- Rokanol K14 as Surface Active Agent (SAA), ethoxylated fatty alcohol, solids content 30 %, pH 5.0–7.0, density 1010 kg·m^{-3}, melting point 303 K, flash point >473 K, (PCC Rokita S.A);
- Silver nitrate ($AgNO_3$), concentration 99.8%, pH 6, density of 4330 kg·m^{-3}, melting point 485 K, boiling point 717 K, (Avantor Performance Materials Poland S.A.);
- Colloidal silica (SiO_2), pH 6–8, density of 2200 kg·m^{-3}, melting point >1700, (Avantor Performance Materials Poland S.A.);
- Acetone, concentration 99.5%, pH 5–6, melting point 178 K, boiling point 329 K, flash point 256 K, density 790 kg·m^{-3}, dynamic viscosity 0.33 mPa·s, (Sigma Aldrich);
- 3-(trimethoxysilyl)-propylamine, boiling point 467 K, flash point 360K, density 1027 kg·m^{-3}, (Sigma Aldrich).

2.2. Methods

2.2.1. Preparation of silver nanoparticles

Silver nanoparticles were prepared with the chemical reduction method. In a typical procedure, about 5 g silica was added into the solution of 0.1712 g of silver nitrate in 5 cm^3 of deionized water and 90 cm^3 acetone. Then, the 5 cm^3 3-(trimethoxysilyl)-propylamine was added into the mixture under continuous stirring at 293 K in order to cross-link the surface of SiO_2. The suspension was stirred for 10 min to deposit silver on colloidal silica. The solution was then filtered through a notched filter. The residue of AgNPs on the filter was dried at 353 K. A crushed, powdered silica with AgNPs was obtained.

2.2.2. Preparation of composite films

The preparation of composite films containing acrylic resin (Alberdingk AC 3640), surfactant (SAA), colloidal silica (SiO_2), and AgNPs was conducted in two stages. At the first stage, water acrylic dispersions presented in Table 1 were prepared. For this purpose, Alberdingk AC 3640, in this study given the

Table 1. Composition of acrylic dispersion (AC 3640).

Sample No.	Resin [cm^3]	SAA [% (w/w)]	SiO_2 [g]	AgNPs [g]
1	50	2	0.49	–
2	50	6	1.57	–
3	50	10	2.28	–
4	50	2	–	0.49
5	50	6	–	1.57
6	50	10	–	2.28

1. Mass percentage, % (w/w), has been expressed in relation to the polymeric mass.
2. Both in Table 1 and in the further part of this paper, for consideration clarity, the abbreviations applied SAA or/and AgNPs denote systems of SiO_2–SAA and SiO_2–Ag–SAA, respectively.

name acrylic resin (50 cm^3), and weighed amounts of Rokanol T-14 (SAA), SiO_2, AgNPs were placed into a glass vessel of a homogenizer. The stirring of the obtained mixture was carried out for 20 min at room temperature, using IKA Ultra-Turrax T-25 (IKA-Werke GmbH & Co. KG, Germany) laboratory homogenizer, IKA-S25N-18G (IKA-Werke GmbH & Co. KG, Germany) mixer with rotational speed equal to $2{\cdot}10^3$ rpm.

The second stage was the formation of films. The film layers for consistometric and thermogravimetric tests were prepared on Petri dishes. The tiles were dried at the temperature of 343 K for 48 hours using SML-30 dryer thermostat (Zalmed, Poland).

For the physical mechanical tests, films applied with an applicator to metal plates – made of S235JR steel type (according to EN 10025) – degreased with n-butyl acetate and mechanically cleaned were used. The samples were then dried at 293 K for seven days.

In order to test the resistance of coatings to liquids, varnish compositions were applied to wooden tiles, which were previously smoothed with sandpaper of K320 (EU Emil Lux, Gmbh&Co.KG, Germany) and covered with a layer of stain (Dragon Sp. z o.o., Skawina, Poland).

2.2.3. Digital light microscope

Microscopic analysis of the AgNPs was performed using a Keyence VHX-7000 digital microscope (Keyence International, Belgium). This technique allowed detailed examination of morphology, particle size and aggregation.

2.2.4. IR spectrum

IR spectroscopic studies of AgNPs samples were carried out using the ALPHA FT-IR spectrometer (Bruker, USA) with a diamond reflection head. Opus 6.5 software was used to record the spectrum: measurement range of 360–44000 cm^{-1}, resolution of 4.0 cm^{-1}. The analysis was done to confirm the existence of a permanent connection between the Ag particles and the SiO_2 carrier, which is essential for successful further research.

2.2.5. Stability assessment

Immediately after the preparation of 50 mL of liquid, samples were placed into flat-bottomed cylindrical glass tubes (height of 55 mm, diameter of 25 mm). Then, the stability of all the emulsions was assessed employing Turbiscan Lab® Expert (Formulation SA, Germany). Basis of this technology is the Static Multiple Light Scattering principle (Sarwar et al., 2021). A source of an infrared light (wavelength $\lambda = 880$ nm) illuminates a sample and two sensors collect the backscattered (BS) and transmitted signals.

Consequently, the Turbiscan Stability Index (TSI) for all compositions as a function of storage time has been evaluated by measurements of the backscattered light intensity at the whole sample height h (Raikos, 2017; Zalewska et al., 2019):

$$\mathrm{TSI} = \sqrt{\frac{\sum_{i=1}^{N} (\mathrm{BS_i} - \mathrm{BS_m})^2}{N-1}} \tag{1}$$

where BS_i and BS_m are the backscattering light intensity obtained in i-th scan ($i = 1, 2, 3, \ldots, N$) and the average arithmetic value of BS_i, respectively, and N is the number of height position in the selected zone of the scans.

The sample can be considered as a stable, when the TSI value tends towards zero.

2.2.6. Particle size distribution

Particle size testing was carried out with the use of the Fritsch Analysette 22 MicroTec Plus laser particle size analyser by Fritsch GmbH (Germany) using the wet method. This consisted of injecting a certain amount of the sample (9 mL) into the device, until adequate flux absorption was achieved. The analyser uses two lasers during measurement. The green laser is responsible for measuring fine particles, while the infrared laser is responsible for analysing large particles. The measurement principle is based on the use of electromagnetic wave scattering. Permissible size of the particles to be determined by means of the analyser should be ranged from 0.5 μm to 1500 μm.

2.2.7. Consistometric measurements

The varnish coatings manufactured were subjected to consistometric tests. The tested material was introduced into a measuring vessel, which was then placed in a Höppler consistometer (VEB MLW Prufgerate-Werk, Germany). A load of 250 g was mounted on top of the device. When the micrometer dial was set to zero, the silicone oil inside the thermostat was began to be heated. As the temperature increased, the sample deformed as expressed by the depth change of the indenter drop. Each change was recorded by the sensor, making it possible to observe the deformations occurring on the micrometer dial to an accuracy of ± 0.01 mm. The experiment was conducted over a temperature range between 303 K and 420 K.

2.2.8. Thermal coating stability

Thermal stability studies of the coatings made of water acrylic emulsions were conducted using a Q1500D derivatograph of the Paulik-Paulik-Erdey system (MON, Hungary). The loss of the sample weight was recorded continuously as the temperature increased to 1273 K at a rate of 5 deg/min in an air

atmosphere. Ceramic crucibles were used. Roasted alumina was the comparative material and also the diluent. The results are presented in the form of a thermogravimetric TG curve presenting the changes in sample mass as a function of temperature, a differential thermogravimetric DTG curve presenting the rate of mass change and establishing the beginning and end of each transformation involving a change in mass, and a curve of a differential thermal analysis DTA indicating exothermic and endothermic reactions occurring in the sample during heating. The thermal effects of thermal decomposition were assessed against the standard, which was benzoic acid. Characteristic temperatures of the phase transformations were determined from the curves and the values of the thermal effects were calculated.

2.2.9. Physicomechanical studies

The quality of the resulting coatings was assessed by marking them:

- thickness using a TestAn DT-856 thickness gauge (Anticorr, Poland) according to the PN-EN ISO 2808;
- relative hardness using the Köenig pendulum apparatus (Anticorr, Poland) according to the PN-EN ISO 1522, measuring the rate of oscillation damping of a physical pendulum with a harder or softer shell at its support point;
- gloss of the coating with a Supergloss 60 glossmeter (Braive Instruments, Belgium) according to the PN EN ISO 2813, measuring angle 60°;
- adhesion using a Peters disc knife (Anticorr, Poland) according to the PN EN ISO 2409, making a grid of incisions and observing the degree of damage to its vertices using a magnifying glass, and
- resistance to sudden deformation according to the DIN EN ISO 6272-2, using the DuPont apparatus (IDM Instruments Pty Ltd., Australia) and determining the greatest height at which no damage to the paint film occurred under impact.

2.2.10. Testing of the coating resistance to liquids

Tests of the resistance of coatings to liquids consisted of evaluating the effects of selected liquids (e.g. water, chemicals, oils, etc.) on the surface changes of the coating, in accordance with the Polish standard PN-EN ISO 2812-4. To do this, a cloth soaked in the test fluid was applied to the coating and protected from drying. After the test, the effects of the liquid on the coating were assessed. The coating destruction assessment follows the scale: no visible changes (5), slight change in gloss and / or colour (4), moderate change in gloss and / or colour (3), a clear change in gloss and / or colour, without changing the surface structure (2), damaged surface, e.g., blisters, partly or completely damaged surface (1). Coatings previously applied to wooden tiles, treated with a layer of wood preservative, were used for the tests.

3. RESULTS AND DISCUSSION

3.1. Digital light microscope

Figure 2 illustrates images of the AgNPs powder (Fig. 2A) and its microscopic image obtained at magnification (×500) (Fig. 2B). The latter photo clearly shows the occurrence of AgNPs agglomerates on the carrier used (indicated in Fig. 2B).

It should be mentioned here that the presence of AgNPs agglomerates adversely affects the stability of the system, but their addition to the polymer emulsion and homogenisation lead to a homogeneous polymer composition (Boivin et al., 2023).

3.2. IR spectrum analysis

The infrared (IR) spectrum of colloidal silica (Fig. 3) on which silver is deposited provides valuable information on the interaction between these materials.

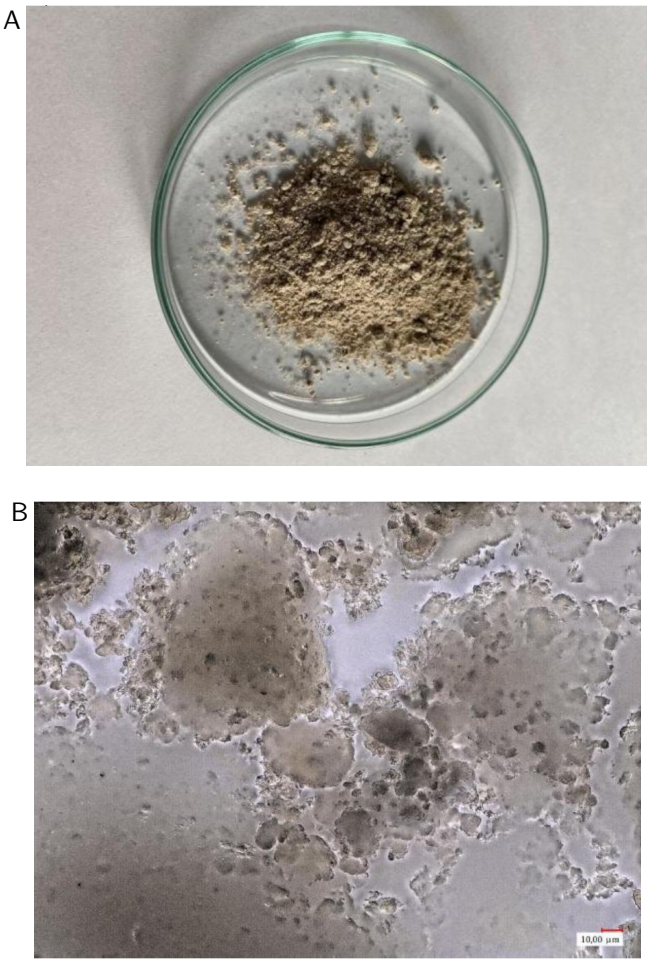

Figure 2. Physical appearance of AgNPs: (A) View of AgNPs after they were completed, (B) Microscope image taken with Keyence VHX-7000 Digital Light Microscope (×500).

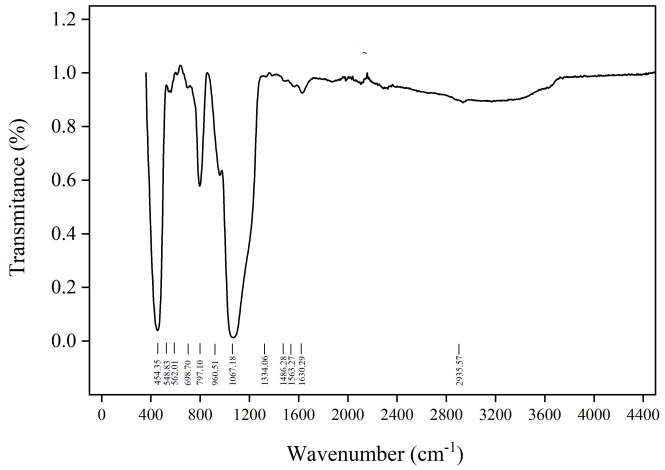

Figure 3. IR spectrum of colloidal silica sample with Ag in the wavelength range 300–4500 cm^{-1}.

By analysing the IR spectrum, it can be seen that the colloidal silica has a strongly developed surface with numerous silanol groups (–SiOH). They represent active sites for nucleation and adsorption of Ag^{+} ions prior to their reduction. Adsorption of silver ions is also favoured by sites with high surface energy. These include surface defects and incompletely condensed siloxane groups (–Si–O–Si–) (Hu et al., 2008). Hence, it can be clearly stated that the presence of vibrations suggests the residues of SiO_2 used to obtain AgNPs. Distinctive IR spectrum bands have been listed in Table 2.

Table 2. Distinctive IR spectrum bands (Fiore and Pellerito, 2021; Smith, 1999).

Analysed signal [cm^{-1}]	Description	Literature value [cm^{-1}]
1630.29	tensile vibrations, C=O	1600–2000
1067.18	asymmetric vibrations Si–O	~ 1090
960.51	asymmetric vibrations Si–OH	~ 950
797.10	symmetric vibrations Si–O	~ 795
454.35	deformation of Si–O–Si	~ 460

3.3. Backscattering analysis

Experimental data describing changes in backscattered light (BS) on the day of preparation and after exposure times of 1, 2, 5, 6, 7 and 14 days for samples with and without AgNPs are shown in Fig. 4

The course of the curves in Fig. 4A clearly shows areas of varying BS intensity, particularly in the lower part of the measuring cell (from 0 to 15 mm). In all cases analysed, there is an increase in the concentration of the dispersed phase in this area as a result of the sedimentation taking place. However, this phenomenon is more noticeable in a system lacking AgNPs.

As can be seen, the longer time, the more stable system is. This is evidenced by the constant BS intensity along the height of the measuring cell and small deviation of its values over time.

Consequently, for cell heights between 15 mm and 45 mm, in practical terms these curves coincide.

More intense changes in the level of BS are revealed in the upper part of the measuring cell (from 45 mm of the height) for systems without AgNPs as well as for systems with an AgNPs content of 2% and 10% (w/w). For example, for the systems without added AgNPs, a sudden increase of BS intensity from 9% for $h = 45$ mm up to 12% for $h = 52$ mm for 2% (w/w) of SAA, from 9% up to 12% for 6% (w/w) of SAA and from 9% to 13% for 10% (w/w) of SAA is shown, which reveals the lack of the system stability, i.e., the creaming phenomenon.

In these systems, for example, a sudden increase of BS intensity from 9% for $h = 45$ mm up to 12% for $h = 52$ mm in the case of 2% (w/w) of AgNPs, and from 8% to 9% for 10% (w/w) of AgNPs is shown, which also reveals the creaming phenomenon.

Only the system with the addition of 6% (w/w) AgNPs demonstrates significant differences (Fig. 4B). In its case it is clear that the addition of AgNPs at 6% (w/w) stabilises the system, as manifested by the uniformity of the BS curves along the measuring cell regardless of the scanning time. Most importantly, backscattering light does not show creaming phenomenon.

In general, it should be noted that the intensity of BS in systems with added AgNPs is significantly lower than in systems without the added modifier. All the analysed water acrylic emulsions are unstable, and the addition of AgNPs improves stability in a noticeable way, especially by the addition of AgNPs in the amount of 6% (w/w). In order to evaluate the stability of the system under consideration, the term 'Turbiscan Stability Index' (hereinafter TSI) has been used and expressed by Eq. (1). The TSI can take values from 0 (stable sample) to 100 (unstable sample), and an increase in its value indicates more intense changes taking place in the system. Thus, by means of the TSI the evaluation of sample stability can be done with a simple method and just one number.

Based on the results presented in this study and obtained using Turbiscan Lab, only samples with TSI values lower than or equal to 4 units can be considered as stable. Such TSI values correspond to the samples with AgNPs content of 6% (w/w) of SAA and containing AgNPs (Fig. 5, black-coloured symbols).

Based on the observation of the TSI values, it can be noted that for all samples not containing AgNPs as well as for the sample containing 2% (w/w) of AgNPs, the TSI values are higher than 11.0, which proves that the dispersions are not stable. In contrast, for emulsions with an AgNPs content of 10% (w/w), the TSI values are slightly lower but too high to

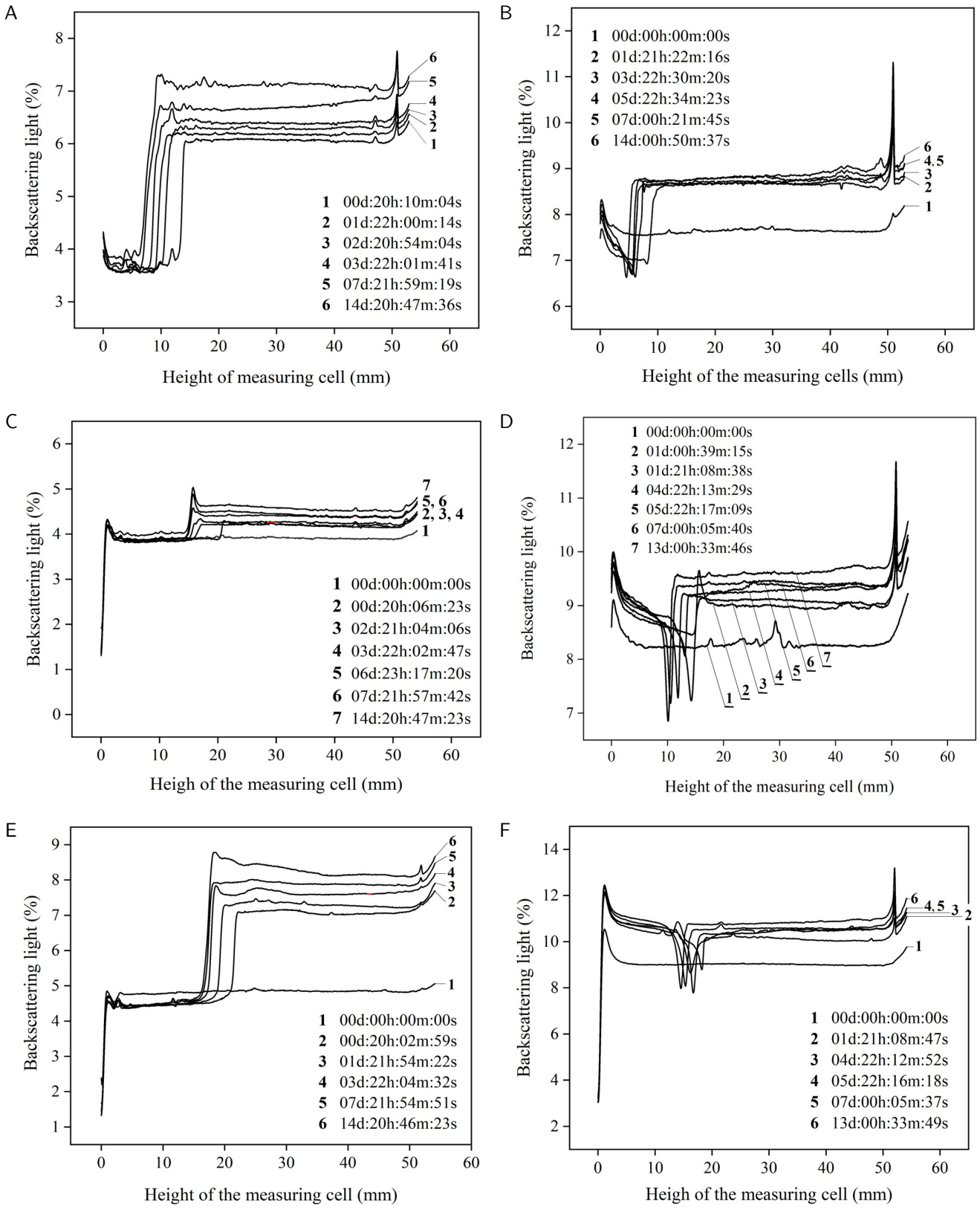

Figure 4. Variation of backscattered light (%) as a function of measuring cell height and exposure time for samples with (A, C, E) and without (B, D, F) silver nanoparticles:
(A) 2% SAA and 2% (w/w) AgNPs, (B) 2% (w/w) SAA, (C) 6% SAA and 6 % (w/w) AgNPs, (D) 6% (w/w) SAA , (E) 10% SAA and 10% (w/w) AgNPs, (F) 10% (w/w) SAA.

consider the produced acrylic dispersion as stable. However, in the case of AgNPs content at the level of 6% (w/w), there is a significant decrease in values of TSI, depending on storage time.

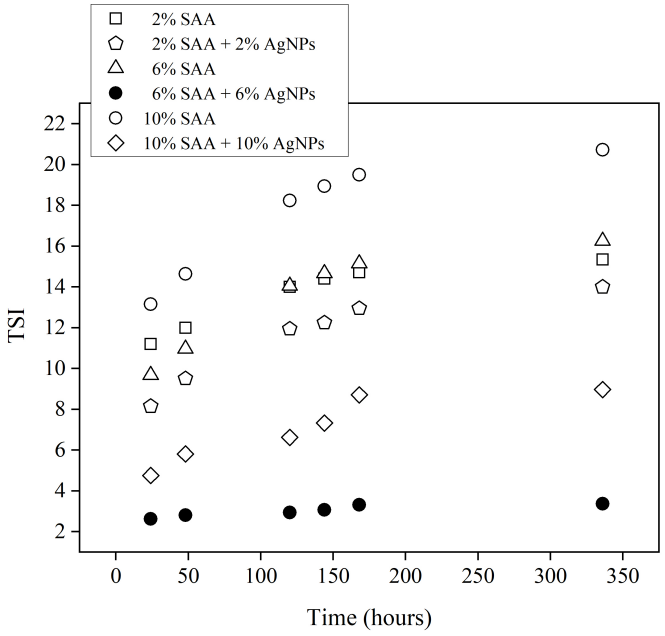

Figure 5. Turbiscan Stability Index (TSI) as a function of storage time for samples listed in Table 1. Black-coloured symbols represent the sample with 6% (w/w) SAA and 6% (w/w) AgNPs content.

This means that, with the total content of AgNPs close to 6% (w/w), a dispersion can be considered stable even after 336 h of storage time and, at the same time, the weight percentage of 6% (w/w) used in the experiment has the highest effectiveness value from the stability viewpoint.

3.4. Analysis of particle size distribution

Diffractometry studies determined the particle size distribution as a function of SAA and AgNPs content in the system at a constant stirrer speed of 15 000 rpm. All samples were analysed at equal intervals. The last measurement was taken on day 14 of preparation. The results of the analysis for a content of both components at 6% (w/w) are shown in Fig. 6.

Particle Size Distribution (PSD) presented in Fig. 6 clearly shows that the addition of AgNPs improves the stability of the polymer dispersion analysed. In systems without added AgNPs (Figs. 6A and 6B), an asymmetrical particle size distribution is noted with an average particle diameter value of approximately 73.7 µm and 70.1 µm, after 1 day and 14 days, respectively. This value is larger than the particle size occurring with the highest probability, indicating a reduced stability of the system compared to the one containing 6% (w/w) AgNPs. In the latter case (Figs. 6C and 6D), the addition of AgNPs

A

LogNormal Model	
Drop diameter (µm)	73.67574 ± 0.90627
Standard deviation (µm)	0.653 ± 0.008
Residual Sum of Squares (µm^{-2})	4.20962
R-Square (COD)	0.99303
Adj. R-Square	0.99280
F Value	4227.7

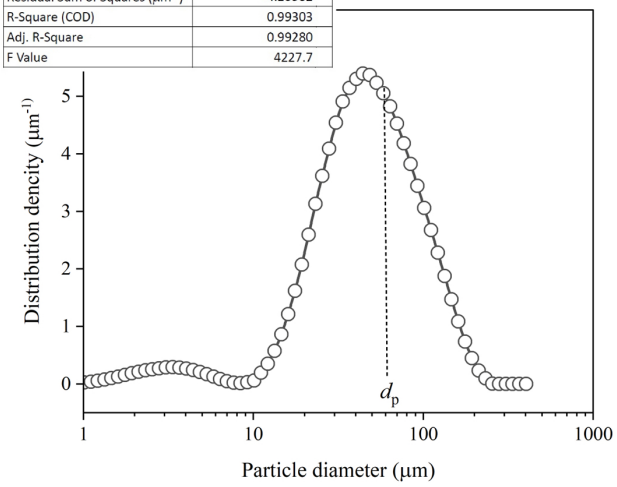

B

LogNormal Model	
Drop diameter (µm)	70.06821 ± 0.97212
Standard deviation (µm)	0.64268 ± 0.00882
Residual Sum of Squares (µm^{-2})	40.99904
R-Square (COD)	0.99071
Adj. R-Square	0.99039
F Value	1771.4

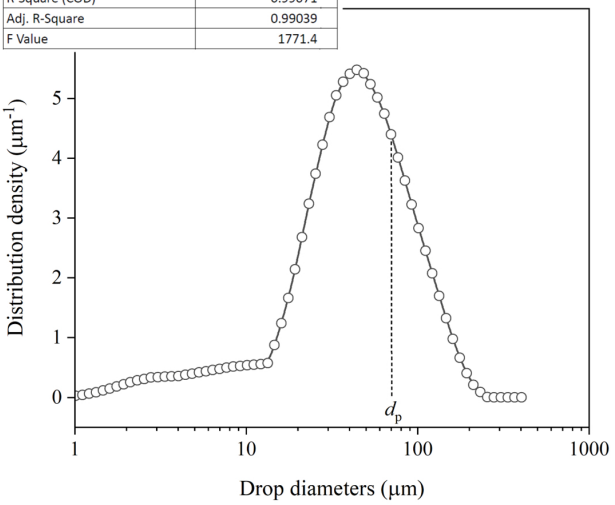

C

LogNormal Model	
Drop diameter (µm)	107.13439 ± 1.67168
Standard deviation (µm)	0.57503 ± 0.01059
Residual Sum of Squares (µm^{-2})	5.87055
R-Square (COD)	0.98345
Adj. R-Square	0.98289
F Value	1762.9

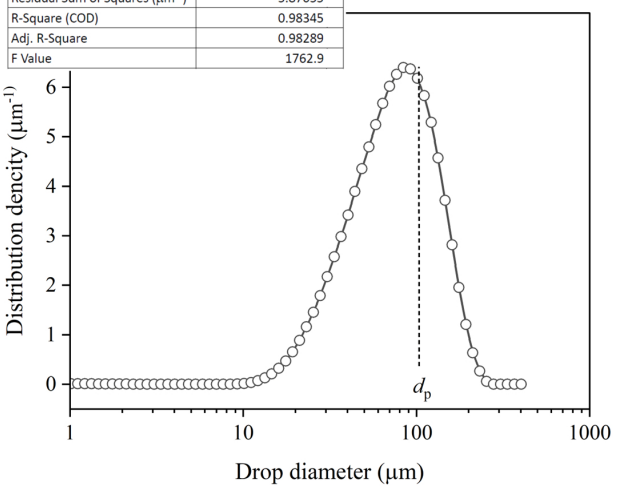

Figure 6 continued at the next page

D

LogNormal Model	
Drop diameter (μm)	101.49715 ± 0.30978
Standard deviation (μm)	0.32588 ± 0.00263
Residual Sum of Squares (μm^{-2})	2.19769
R-Square (COD)	0.99692
Adj. R-Square	0.99682
F Value	9605.1

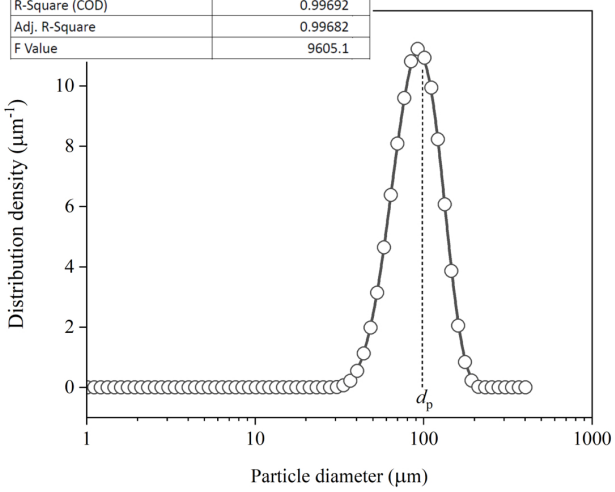

Figure 6. Particle Size Distribution for Alberdindk AC 3640 composition: (A) with 6% (w/w) of SAA after 1 day, (B) with 6% (w/w) of SAA after 14 days, (C) with 6% (w/w) of SAA +6% (w/w) of AgNPs after 1 day, (D) with 6% (w/w) of SAA +6% (w/w) of AgNPs after 14 days.

makes the distributions symmetrical with an average particle diameter value of about 107.1 μm and 101.5 μm, after 1 day and 14 days, respectively, and close to those most common ones in the set. The increase in diameter can be explained by the formation of micelles, which increase the stability of the system. The high F-values demonstrate the excellent fit of the log-normal model to the experimental, discrete distribution. Smaller scatter of particle diameters is also observed after the addition of AgNPs.

3.5. Consistometric test results

As a result of the tests carried out with the use of a consistometer, deformation diagrams were drawn up as a function of temperature (Fig. 7).

The waveforms presented (Fig. 7A) differ in the value of deformation expressed in millimetres per one degree of temperature change, $\Delta D/\Delta T$ (mm·deg^{-1}), as shown in Fig. 7B. From a performance point of view, it is beneficial for the change rate to be as low as possible.

For each of the curves shown in Fig. 7A, three temperature ranges can be distinguished that differentiate the courses of the deformation curves and thus the behaviour of the produced coatings: 1) up to 320 K, 2) between 320 K and 350 K, and 3) above 350 K.

The first range demonstrates characteristic deformational changes due to temperature changes. As can be seen from the graph, these slowed deformation changes (increased thermomechanical stability (TMS)) are the result of the addition of AgNPs in amounts greater than 2% (w/w). Then, the formation of internal bonds between the individual components takes place, which hinders the flow of the polymer segments in the membrane, shifting the adverse effect of temperature towards higher temperature values. It is evident that coatings without the addition of AgNPs lose their thermomechanical stability faster at temperatures below 320 K than do coatings with AgNPs.

In the second range, i.e., for temperatures from 320 K to about 350 K, an increase in deformation is noted, indicating a decrease in coating stability. However, the stabilising effect of the addition of AgNPs is evident in this range, causing a decrease in the deformation rate $\Delta D/\Delta T \cdot 10^3$ (mm·deg^{-1})

A

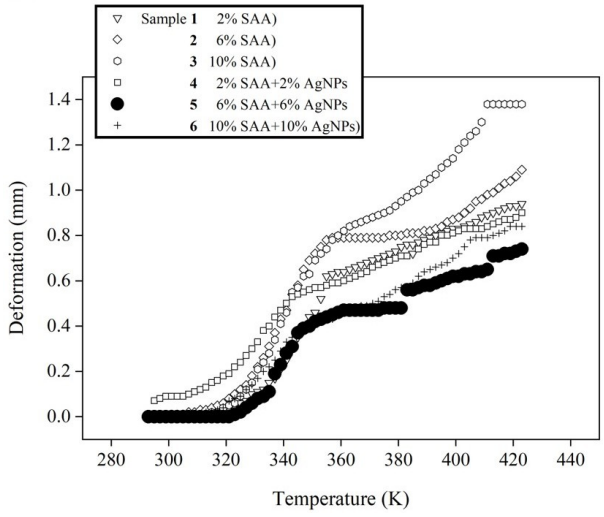

B

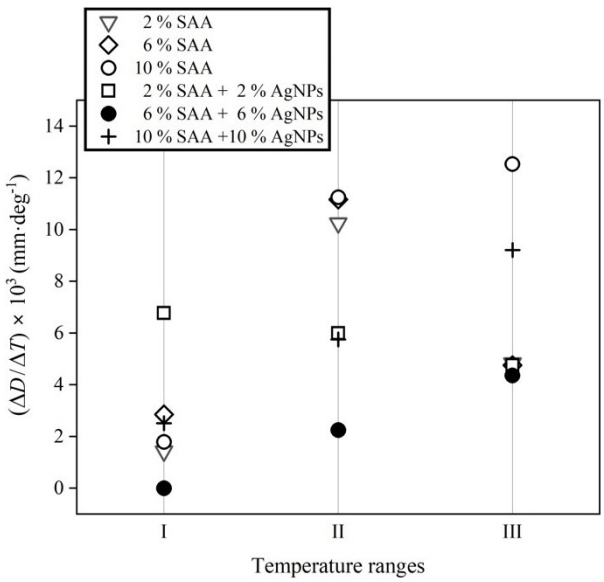

Figure 7. (A) Coating deformation D as a function of temperature T for samples without and with addition of AgNPs, (B) Values of the indicator $\Delta D/\Delta T$ in the specified during the deformation temperatures ranges. The black-coloured symbol represents the samples with the lowest deformation rate.

Table 3. Results of thermogravimetric test.

Sample no.	AC 3640 Sample		Process Type	T_i [K]	T_f [K]	T_{max} [K]	ΔH [kJ/g]
	SAA [% (w/w)]	AgNPs [% (w/w)]					
1	2	–	endothermic	555	666	645	–0.79
	2	–	exothermic	665	749	685	0.70
2	6	–	endothermic	570	653	623	–0.47
	6	–	exothermic	651	770	692	1.30
3	10	–	endothermic	569	661	638	–0.68
	10	–	exothermic	570	852	690	1.69
4	2	2	endothermic	570	654	620	–0.48
	2	2	exothermic	656	784	684	1.04
5	6	6	endothermic	570	659	630	–0.60
	6	6	exothermic	660	778	692	1.32
6	10	10	endothermic	566	660	641	–0.66
	10	10	exothermic	661	988	693	2.06

from 10.25, 11.16 and 11.25, in the case of the addition of 2% (w/w) SAA, 6% SAA (w/w) and 10% SAA (w/w), respectively, to 6, 2.25 and 5.75, in the case of the addition of AgNPs in the aforementioned amounts, respectively.

The third range, i.e., temperatures higher than 350 K, sees a slight decrease in deformation increase $\cdot\Delta D/\Delta T10^3$ (mm·deg^{-1}) from 4.84, 4.76 and 12.53 when only SAA is added at 2%, 6% and 10% (w/w), respectively, to 4.76, 4.36 and 9.2 when AgNPs are added at 2%, 6% and 10% (w/w), respectively. Although the increment values $\cdot\Delta D/\Delta T10^3$ may vary slightly, the actual deformation values in Fig. 7 show a decreasing trend with the addition of AgNPs, particularly pronounced after the addition of AgNPs at 6% (w/w).

Figure 8 shows the differences between the flow temperatures, T_P, and softening temperatures, T_S. Between the temperatures of softening, T_S and flowing, T_P, the coating becomes more susceptible to deformation, and can soften and lose its original form. Above the flow temperature T_P, the tested sample loses its structure completely and becomes liquid. Thus, the temperature values obtained (T_S and T_P) allowed an assessment to be made of the temperature range over which the coatings tested retain their functional properties. The higher the values of the analysed temperatures T_S and T_P, the more thermally stable the coating is, as it retains its rigidity and mechanical strength.

According to the results shown in Fig. 8, it can be concluded that the addition of AgNPs reduces the temperature range over which the membrane is susceptible to deformation. At the same time, the value of the film-softening temperature T_S increases, which has a beneficial effect on the durability and thermal stability of the coating produced (samples 4–6).

Thus, also the results of the consistometric tests showed that the addition of AgNPs at 6% (w/w) causes the least deformation of the analysed polymer compositions while ensuring their thermomechanical stability.

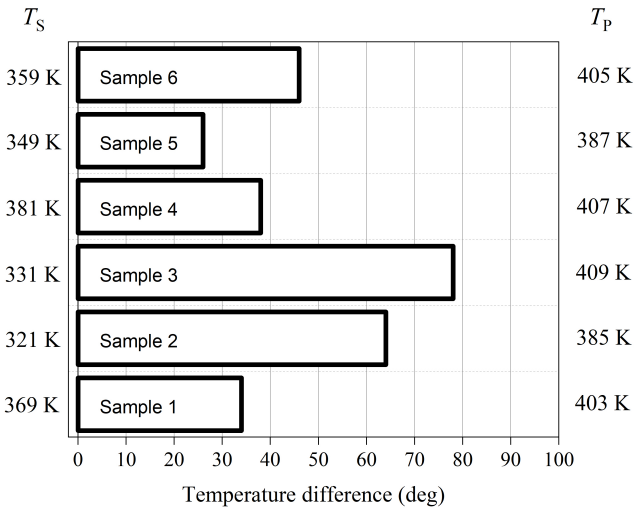

Figure 8. Filming temperature range: T_S and T_P denote the softening temperature and the pour point, respectively.

3.6. Derivatographic test results

Figure 9 shows the results of thermogravimetric decomposition tests for varnish compositions without and with the addition of 6% (w/w) AgNPs.

From the curves shown, it can be seen that the thermal decomposition process of the varnish composition takes place in two stages and is either exothermic or endothermic. From the DTG, DTA and TG curves, initial temperatures (T_i), maximum decomposition rate temperatures (T_{max}), and final transformation temperatures (T_f) were determined, and the heat effects were calculated (ΔH). The results are summarised in Table 3 (Chattopadhyay et al., 2004).

The above diagrams show, for both samples analysed above, that an initial mass loss caused by the presence of volatiles and moisture and impurities is observed (around 530 K), followed by the actual degradation process initiated at a temperature

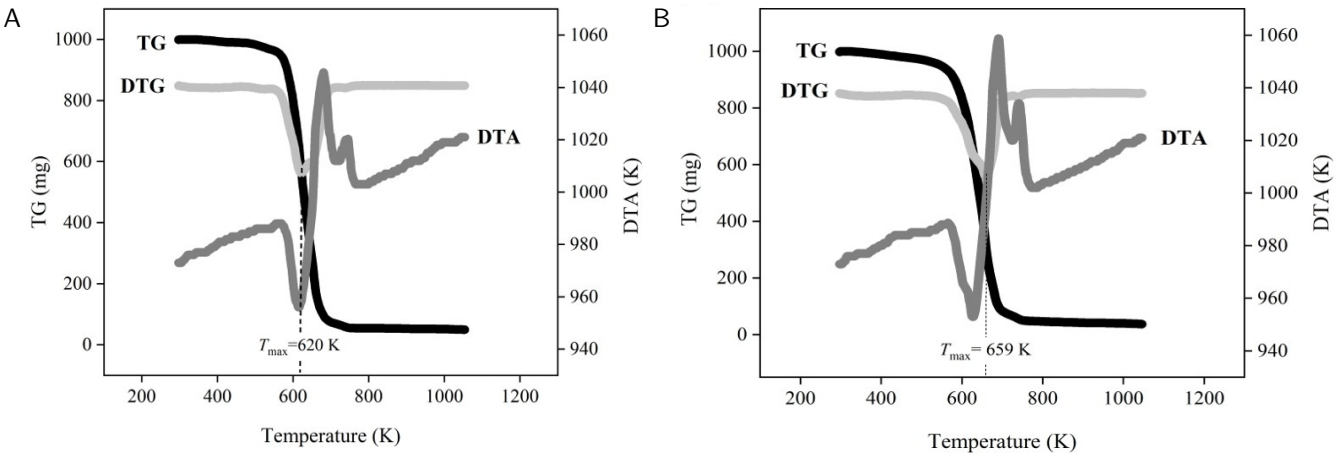

Figure 9. Exemplary results of thermogravimetric analysis (TGA): (A) with 6% (w/w) of SAA, (B) with 6 % (w/w) of SAA + 6% (w/w) of AgNPs.

T_i, contained in the range 566 K to 570 K (Table 3), with one exception relating to the sample with 6% (w/w) SAA, for which T_i = 555 K. The final degradation temperature T_f for all the aqueous acrylic dispersions analysed adopts values between 653 K and 660 K, while the temperature T_{max}, corresponding to the maximum degradation rate and derived from the extreme point coordinates, reaches values between 620 K and 659 K (Fig. 10).

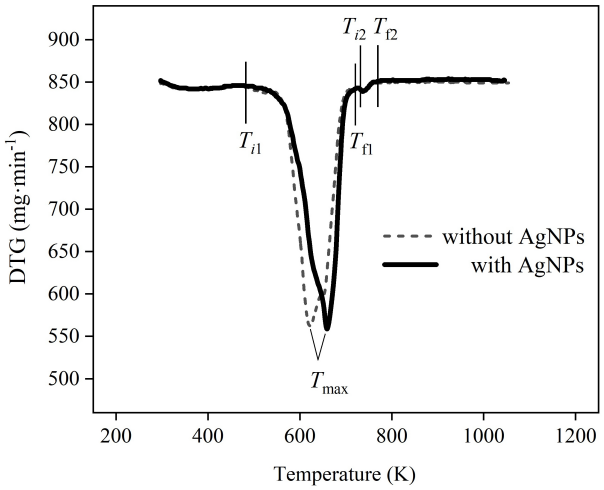

Figure 10. Differential thermogravimetry curves (DTG) with (solid line) and without (dashed line) AgNPs, corresponding the samples presented in Figs. 9A and 9B. $T_{i,j}$ and $T_{f,j}$, $j = 1, 2$) denote the initial and final decomposition temperatures, respectively.

Thus, when the AgNPs have been added, the analysed polymer composition degrades more slowly and requires a higher temperature to reach the decomposition maximum rate.

On the other hand, when analysing the differential thermal analysis (DTA) curve, one notices the occurrence of intense maxima and minima, responsible for exothermic and endothermic transformations respectively. It can be seen that the former (exothermic transformations), associated with oxidation of the decomposition products or the polymer itself, occur at temperatures of about 580 K, 700 K and 730 K, while the endothermic transformations represented by the thermal decomposition of the individual components of the dispersion correspond to temperatures of about 620 K, 720 K and 800 K. Furthermore, it can be seen that an increase in the content of SAA and AgNPs intensifies the thermal effect of the transformations, a consequence caused by an increase in the amount of the individual modifiers of the acrylic polymer composition.

Thus, it can be clearly stated on the basis of the thermogravimetric analysis carried out (Figs. 9A and 9B), that the addition of both SAA and AgNPs to the acrylic polymer compositions analysed does not significantly affect the waveform of the thermogravimetric curves, causing only a shift of the decomposition maximum rate temperature (T_{max}) toward higher values, which indicates a stabilizing effect on the investigated system.

3.7. Physicomechanical study results

The results of the physical-mechanical tests are given in Figs. 11 and 12. As can be seen there, the addition of AgNPs contributes to the improvement of physical-mechanical properties, i.e., the higher the mass fraction of AgNPs added, the more favourable properties are obtained.

By analysing the relative hardness (Fig. 11) – expressed as the quotient of the pendulum oscillation damping time with the support point located on the surface of the test coating and the pendulum oscillation damping time with the support point located on a reference glass plate – the addition of a surfactant (SAA) increases the Koenig pendulum's oscillation damping time, resulting in an increase in relative hardness to 0.38 for an SAA content of 10% (w/w).

The addition of AgNPs strengthens the polymer network formed by SAA and induces an additional increase in relative hardness, which for 10% (w/w) AgNPs content is 0.56.

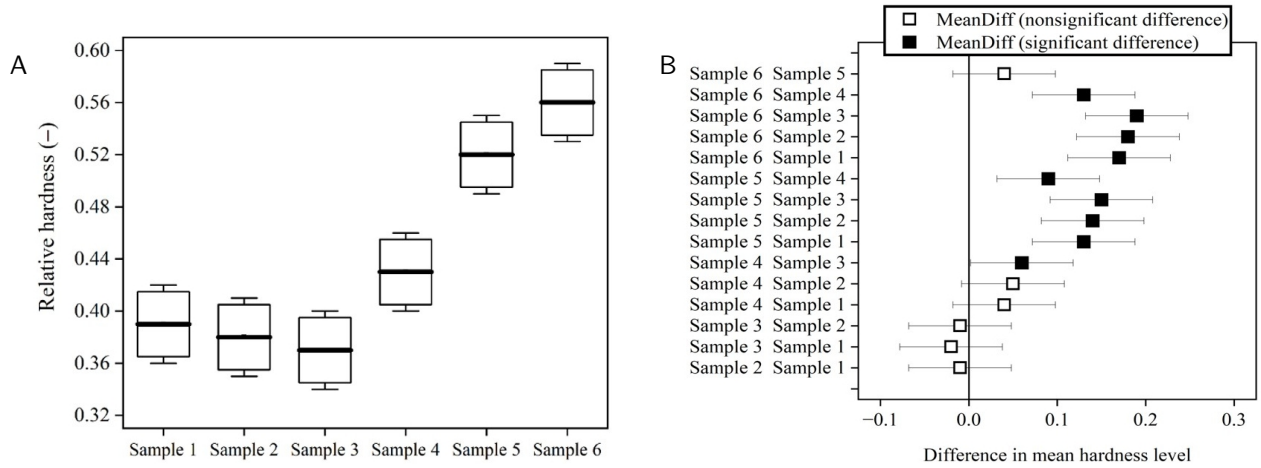

Figure 11. (A) Relative hardness of coatings for samples under considerations, (B) Graphical interpretation of Tukey's test.

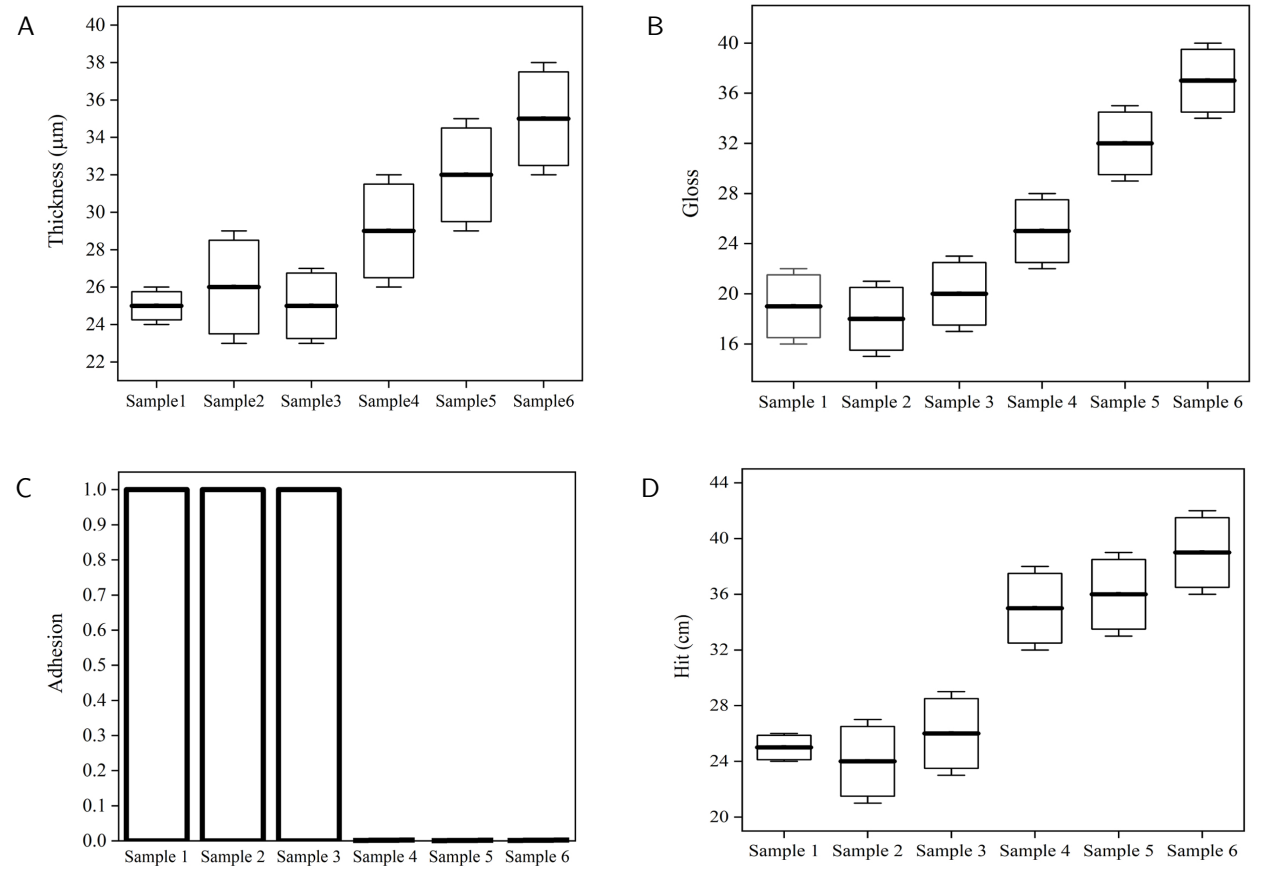

Figure 12. Assessment of thermomechanical properties of coatings for samples listed in Table 1.

A similar effect is noted for the other analysed properties shown in Fig. 12 In the case of gloss, the addition of 10% (w/w) of AgNPs increases the value from 20 to 37; in the case of impact resistance (Fig. 12D), there is an increase from 0.26 m to 0.39 m, and in the case of thickness, it increases from 29 µm to 35 µm, which from a practical point of view can be considered a stable value. Noteworthy is the adhesion of the coating, which takes two values, i.e., 1 (the total area of the damaged coating is not greater than 5%) and 0 (the coating shows adhesion, no square of the notch grid has been torn off). This property has also been improved with the addition of AgNPs.

The results illustrated in Figs. 11A and 12 (except for Fig. 12C) have been confirmed by ANOVA with Tukey's (Honestly Significant Difference) test (Fig. 11B), which allows us to compare averages across samples and determine whether the differences in their values are statistically significant.

The test shows that statistically significant differences exist between samples containing 6% and 10% (w/w) AgNPs (Samples 5 and 6), as well as samples 4 with 2% (w/w) AgNPs and without AgNPs.

Identical analyses were performed for each thermomechanical property studied. It can be seen that the higher the content of AgNPs, the better properties can be expected.

3.8. Resistance of coatings to liquids

Alberdingk AC 3640 resin-based coatings, both without and with modifiers (SAA, AgNPs), show excellent resistance (no visible changes (5), slight change in gloss and / or colour (4)) to wine. Resistance to wine is particularly important for kitchen furniture or tables. All the tested coatings withstand contact with liquids such as water, oil, and boiling water very well.

Acetone, on the other hand, is aggressive in all cases, causing complete damage to the coating, so contact of the furniture with this liquid should be avoided.

Coffee and tea cause slightly less damage than acetone, but still have an adverse effect on coatings. The addition of AgNPs did not significantly improve fluid resistance. Instead, it can provide additional properties such as antibacterial action, which is beneficial in some applications (Le et al., 2019).

Table 4. Summary of the results from the test of resistance of coatings to liquids.

		Sample number					
		1	2	3	4	5	6
Type of fluid	Time of action	The coating destruction assessment on a scale of 1 to 5					
CIF cleaning cream	16 h	3	2	4	3	2	4
ethanol of 96%	16 h	4	4	4	1	3	4
wine	16 h	4	5	5	5	5	4
coffee	16 h	5	5	2	4	2	4
tea	16 h	5	5	3	4	5	4
edible oil	24 h	5	5	5	5	5	5
water	24 h	5	5	5	5	5	5
acetone	10 s	1	1	1	1	1	1
acetone	1 min	1	1	1	1	1	1
boiling water	pouring	5	5	5	5	5	5

The coating destruction assessment is scaled as follows: no visible changes (5), slight change in gloss and / or colour (4), moderate change in gloss and / or colour (3), a clear change in gloss and / or colour, without changing the surface structure (2), damaged surface, e.g., blisters, partly or completely damaged surface (1)

As shown above, the content of SAA and AgNPs in the range of the tested concentrations has a significant effect on the physical-mechanical properties of the coatings and leads to significant improvements of these properties. This, in turn, translates into better surface protection against mechanical damage and weathering.

4. CONCLUSIONS

This paper presents findings about the effect of the silver nanoparticle (AgNPs) concentration on the stability of water-based acrylic emulsions and thermomechanical properties of coatings made of them, considering AgNPs content of 2%, 6% and 10% (w/w).

The analysis performed in this paper enables to draw the following conclusions that may be helpful in selection of technological conditions in industrial practice:

- For all water-based acrylic dispersions containing only surfactant (SAA) at 2%, 6% and 10% (w/w), the Turbiscan Stability Index values increase with the increasing amount of SAA, rising to values above 11. The opposite behaviour is reported for the dispersions containing AgNPs, i.e., the TSI values decrease with an increase in the AgNPs content. However, there exists the content of 6% (w/w) of AgNPs for which the water acrylic dispersion can be considered stable.
- All systems containing only the surfactant showed instability revealed by expected sedimentation and migration of the dispersed phase leading to the creaming phenomenon. Although the addition of AgNPs slightly stabilises the systems studied, the phenomena mentioned also occur after the addition of AgNPs at 2% and 10% (w/w). Only the addition of AgNPs at 6% (w/w) eliminates the unfavourable creaming phenomenon by stabilising the water-based acrylic emulsions over time and along the depth of the emulsion layer.
- The thermogravimetric analysis showed that the addition of AgNPs did not significantly affect the waveform of the thermogravimetric curves, causing only a shift of the decomposition maximum rate temperature (T_{max}) toward higher values, which demonstrates the stabilizing effect of silver nanoparticles on the system under consideration.
- The addition of silver nanoparticles to water acrylic emulsions – after film solidification – results in an improved relative hardness, impact resistance, coating adhesion and gloss. The more AgNPs the emulsion contains, the more favourable thermomechanical indices are achieved. The content of AgNPs in aqueous acrylic compositions did not significantly improve the resistance of resulting coatings to liquids present in everyday life.
- The most stable system was the water acrylic emulsion containing 6% (w/w) of SAA and 6% (w/w) of AgNPs. For the mentioned weight contents of both modifiers, the particle size distributions become symmetrical, compared

to the sample without AgNPs, so that the average value of the volume equivalent diameter increases and corresponds to the value of the most probable diameter in the system.
- The analysis presented in this study advances the understanding of how silver nanoparticle (AgNPs) content affects the stability of water-based acrylic dispersions and the thermomechanical properties of the resulting coatings. Comprehending and predicting phenomena such as aggregation and supersaturation induced by the presence of AgNPs is crucial for the design and optimization of compatible carrier systems. It also highlights the technological challenge of determining the optimal concentrations of both emulsifiers and AgNPs. The ability to anticipate changes in coating materials based on experimental data is highly valuable in engineering practice. Therefore, the findings of this study can be used to minimize the need for extensive experimental procedures prior to the successful application of water-based acrylic emulsions in various areas of life.

SYMBOLS

D	deformation, mm
T	temperature, K
T_i	transformation initial temperature, K
T_f	transformation final temperature, K
T_{max}	temperature of the decomposition maximum rate
T_P	pour point, K
T_S	softening temperature, K
AgNPs	Silver nanoparticles,
BS	Backscattering light
DTA	Differential Thermal Analysis
DTG	Differential Thermal Gravimetry
PSD	Particle Size Distribution
SAA	Surface Active Agent (emulsifier)
TG	Thermal Gravimetry
TMS	Thermomechanical Stability
TSI	Turbiscan Stability Index

REFERENCES

Abazari M., Badeleh S.M., Khaleghi F., Saeedi M., Haghi F., 2023. Fabrication of silver nanoparticles-deposited fabrics as a potential candidate for the development of reusable facemasks and evaluation of their performance. *Sci. Rep.*, 13, 1593. DOI: 10.1038/s41598-023-28858-9

Abdullayev E., Price R., Shchukin D., Lvov Y., 2009. Halloysite tubes as nanocontainers for anticorrosion coating with benzotriazole. *ACS Appl. Mater. Interfaces*, 1, 1437–1443. DOI: 10.1021/am9002028

Akbarian M., Olya M.E., Ataeefard M., Mahdavian M., 2012. The influence of nanosilver on thermal and antibacterial properties of a 2K waterborne polyurethane coating. *Prog. Org. Coat.*, 75, 344–348. DOI: 10.1016/j.porgcoat.2012.07.017

Apelfeld A., Grigoriev S., Krit B., Ludin V., Suminov I., Chudinov D., 2022. Improving the stability of the coating properties for group plasma electrolytic oxidation. *Manuf. Lett.*, 33, 54–59. DOI: 10.1016/j.mfglet.2022.08.005

Assis M., Simoes L.G.P., Tremiliosi G.C., Ribeiro L.K., Coelho D., Minozzi D.T., Santos R.I., Vilela D.C.B., Mascaro L.H., Andrés J., Longo E., 2021. PVC-SiO_2-Ag composite as a powerful biocide and anti-SARS-CoV-2 material. *J. Polym. Res.*, 28, 361. DOI: 10.1007/s10965-021-02729-1

Benitha V.S., Jeyasubramanian K., Prabhin V.S., Dhanabalan S., Thirumurugan A., 2024. Chapter 26 - Nanomaterials in paints, In: Malik M.I., Hussain D., Shah M.R., Guo D.-S. (Eds.), *Handbook of nanomaterials, Volume 1*. Elsevier, 693–720. DOI: 10.1016/B978-0-323-95511-9.00024-X

Boivin G., Ritcey A.M., Landry V., 2023. Silver nanoparticles as antifungal agents in acrylic latexes: Influence of the initiator type on nanoparticle incorporation and *Aureobasidium pullulans* resistance. *Polymers*, 15, 1586. DOI: 10.3390/polym15061586

Carbone M., Donia D.T., Sabbatella G., Antiochia R., 2016. Silver nanoparticles in polymeric matrices for fresh food packaging. *J. King Saud Univ. Sci.*, 28, 273–279. DOI: 10.1016/j.jksus.2016.05.004

Chattopadhyay D.K., Rohini Kumar D.B., Sreedhar B., Raju K.V.S.N., 2004. Thermal stability and dynamic mechanical behavior of acrylic resin and acrylic melamine coatings. *J. Appl. Polym. Sci.*, 91, 27–34. DOI: 10.1002/app.13145

Chinh N.T., Dao P.H., Vu Q.T., Nguyen A.H., Nguyen X.T., Ly T.N.L., Tran T.K.N., Hoang T., 2022. Assessment of characteristics and weather stability of acrylic coating containing surface modified zirconia nanoparticles. *Prog. Org. Coat.*, 163, 106675. DOI: 10.1016/j.porgcoat.2021.106675

Dhaka A., Chand Mali S., Sharma S., Trivedi R., 2023. A review on biological synthesis of silver nanoparticles and their potential applications. *Results Chem.*, 6, 101108. DOI: 10.1016/j.rechem.2023.101108

Duman H., Eker F., Akdaşçi E., Witkowska A.M., Bechelany M., Karav S., 2024. Silver nanoparticles: A comprehensive review of synthesis methods and chemical and physical properties. *Nanomaterials*, 14, 1527. DOI: 10.3390/nano14181527

Fiore T., Pellerito C., 2021. Infrared absorption spectroscopy, In: Agnello S. (Ed.), *Spectroscopy for materials characterization*. John Wiley & Sons, Inc., 129–167. DOI: 10.1002/9781119698029.ch5

Gherasim O., Puiu R.A., Bîrcă A.C., Burdușel A.-C., Grumezescu A.M., 2020. An updated review on silver nanoparticles in biomedicine. *Nanomaterials*, 10, 2318. DOI: 10.3390/nano10112318

Gómez-Ortíz N., De la Rosa-García S., González-Gómez W., Soria-Castro M., Quintana P., Oskam G., Ortega-Morales B., 2013. Antifungal coatings based on $Ca(OH)_2$ mixed with ZnO/TiO_2 nanomaterials for protection of limestone monuments. *ACS Appl. Mater. Interfaces*, 5, 1556–1565. DOI: 10.1021/am302783h

Hoang V.-T., Mai M., Le T.T., Vu N.P., Nguyen T.K., Phuong D.T., Tran Q.H., Le A.-T., Ngo X.D., Tran V.-H., 2020. Functionalized-AgNPs for long-term stability and its applicability in the detection of manganese ions. *Adv. Polym. Technol.*, 2020, 9437108. DOI: 10.1155/2020/9437108

Hu J., Ma J., Deng W., 2008. Properties of acrylic resin/nano-SiO_2 leather finishing agent prepared via emulsifier-free emulsion polymerization. *Mater. Lett.*, 62, 2931–2934. DOI: 10.1016/j.matlet.2008.01.127

Kargozar S., Mozafari M., 2018. Nanotechnology and nanomedicine: Start small, think big. *Mater. Today Proc.*, 5, 15492–15500. DOI: 10.1016/j.matpr.2018.04.155

Keijzer P.H., de Jongh P.E., de Jongh K.P. 2022. Utilization of silver silicate for the formation of highly dispersed silver on silica catalysts. *ChemCatChem*, 14, e202101702. DOI: 10.1002/cctc.202101702

Khan M.R., Urmi M.A., Kamaraj C., Malafaia G., Ragavendran C., Rahman M.M., 2023. Green synthesis of silver nanoparticles with its bioactivity, toxicity and environmental applications: A comprehensive literature review. *Environ. Nanotechnol. Monit. Manage*, 20, 100872. DOI: 10.1016/j.enmm.2023.100872

Le T.T., Nguyen T.V., Nguyen T.A., Huong N.T.T., Thai H., Tran D.L., Dinh D.A., Nguyen T.M., Lu L.T., 2019. Thermal, mechanical and antibacterial properties of water-based acrylic Polymer/SiO_2–Ag nanocomposite coating. *Mater. Chem. Phys.*, 232, 362–366. DOI: 10.1016/j.matchemphys.2019.05.001

Loiseau A., Asila V., Boitel-Aullen G., Lam M., Salmain M., Boujday S., 2019. Silver-based plasmonic nanoparticles for and their use in biosensing. *Biosensors*, 9, 78. DOI: 10.3390/bios9020078

Manjumeena R., Venkatesan R., Duraibabu D., Sudha J., Rajendran N., Kalaichelvan P.T., 2016. Green nanosilver as reinforcing eco-friendly additive to epoxy coating for augmented anticorrosive and antimicrobial behavior. *Silicon*, 8, 277–298. DOI: 10.1007/s12633-015-9327-2

Mousavi M., Fini E., 2020. Silanization mechanism of silica nanoparticles in bitumen using 3-aminopropyl triethoxysilane (APTES) and 3-glycidyloxypropyl trimethoxysilane (GPTMS). *ACS Sustainable Chem. Eng.*, 8, 3231–3240. DOI: 10.1021/acssuschemeng.9b06741

Ong W.T.J., Nyam K.L., 2022. Evaluation of silver nanoparticles in cosmeceutical and potential biosafety complications. *Saudi J. Biol. Sci.*, 29, 2085–2094. DOI: 10.1016/j.sjbs.2022.01.035

Piracha S., Saleem S., Momil, Basharat G., Anjum A., Yaseen Z., Saleem S., 2021. Nanoparticle: Role in chemical industries, potential sources and chemical catalysis applications. *Sch. Int. J. Chem. Mater. Sci.*, 4, 40–45. DOI: 10.36348/sijcms.2021.v04i04.006

Raikos V., 2017. EDOIncapsulation of vitamin E in edible orange oil-in-water emulsion beverages: Influence of heating temperature on physicochemical stability during chilled storage. *Food Hydrocolloids*, 72, 155–162. DOI: 10.1016/j.foodhyd.2017.05.027

Sarmast M.K., Salehi H., 2016. Silver nanoparticles: An influential element in plant nanobiotechnology. *Mol. Biotechnol.*, 58, 441–449. DOI: 10.1007/s12033-016-9943-0

Sarwar A., Aziz T., Al-Dalali S., Zhang J., Din J.U., Chen C., Cao Y., Fatima H., Yang Z., 2021. Characterization of synbiotic ice cream made with probiotic yeast *Saccharomyces boulardii* CNCM I-745 in combination with inulin. *LWT*, 141, 110910. DOI: 10.1016/j.lwt.2021.110910

Sati A., Ranade T.N., Mali S.N., Ahmad Yasin H.K., Pratap A., 2025. Silver nanoparticles (AgNPs): Comprehensive insights into bio/synthesis, key influencing factors, multifaceted applications, and toxicity – A 2024 update. *ACS Omega*, 10, 7549–7582. DOI: 10.1021/acsomega.4c11045

Schaming D., Remita H., 2015. Nanotechnology: from the ancient time to nowadays. *Found. Chem.*, 17, 187–205. DOI: 10.1007/s10698-015-9235-y

Schluesener J.K., Schluesener H.J., 2013. Nanosilver: application and novel aspects of toxicology. *Arch. Toxicol.*, 87, 569–576. DOI: 10.1007/s00204-012-1007-z

Şen F., Kocatürk E., ÇakmakçıE., Kahraman M.V., 2022. Quaternary imidazolium-functionalized reactive silica nanoparticles-containing thiol-ene photocured antibacterial hybrid coatings. *React. Funct. Polym.*, 170, 105149. DOI: 10.1016/j.reactfunctpolym.2021.105149

Shah M.A., Pirzada B.M., Price G., Shibiru A.L., Qurashi A., 2022. Applications of nanotechnology in smart textile industry: A critical review. *J. Adv. Res.*, 38, 55–75. DOI: 10.1016/j.jare.2022.01.008

Shahzadi S., Fatima S., Ul Ain Q., Shafiq Z., Janjua M.R.S.A., 2025. A review on green synthesis of silver nanoparticles (SNPs) using plant extracts: a multifaceted approach in photocatalysis, environmental remediation, and biomedicine. *RSC Adv.*, 15, 3858–3903. DOI: 10.1039/D4RA07519F

Sharma B., Singh S., Prakash B., Sharma H., Maji P.K., Dutt D., Kulshreshtha A., 2022. Effect of cellulose nanocrystal incorporated acrylic copolymer resin on printing properties of waterborne inks. *Prog. Org. Coat.*, 167, 106842. DOI: 10.1016/j.porgcoat.2022.106842

Sharma K., Singh G., Kumar M., Bhalla V., 2015. Silver nanoparticles: facile synthesis and their catalytic application for the degradation of dyes. *RSC Adv.*, 5, 25781–25788. DOI: 10.1039/C5RA02909K

Smith B.C., 1999. *Infrared spectral interpretation: A systematic approach*. 1st edition, CRC Press. DOI: 10.1201/9780203750841

Taran M., Safaei M., Karimi N., Almasi A., 2021. Benefits and application of nanotechnology in environmental science: an overview. *Biointerface Res. Appl. Chem.*, 11, 7860–7870. DOI: 10.33263/BRIAC111.78607870

Tornero A.C.F., Blasco M.G., Azqueta M.C., Fernández-Acevedo C., Salazar-Castro C., López S.J.R., 2018. Antimicrobial ecological waterborne paint based on novel hybrid nanoparticles of zinc oxide partially coated with silver. *Prog. Org. Coat.*, 121, 130–141. DOI: 10.1016/j.porgcoat.2018.04.018

Wu X., Zhou Z., Wang Y., Li J., 2020. Syntheses of silver nanowires ink and printable flexible transparent conductive film: A review. *Coatings*, 10, 865. DOI: 10.3390/coatings10090865

Zalewska A., Kowalik J., Grubecki I., 2019. Application of turbiscan lab to study the effect of emulsifier content on the stability of plant origin dispersion. *Chem. Proc. Eng.*, 40, 399–409. DOI: 10.24425/cpe.2019.130214

Zhang C., Ren X., Cui X., Bai H., Zhang X., Li H., 2021. SiO_2 nanoparticles modified by bridged polysilsesquioxane-based protective coatings for moisture proofing and antireflection applications. *ACS Appl. Nano Mater.*, 4, 12137–12145. DOI: 10.1021/acsanm.1c02670